Mongolian Journal of Chemistry
www.mongoliajol.info/index.php/MJC

# Development of a polymer resin immobilized catalysts for the oxidative transformation of ethylbenzene

Sunil Kumar[1], Praveen Kumar Gupta[1]✉, Amit Kumar[2] and Ramesh Kumar[3]

[1]*Department of Chemistry, Maharishi Markandeshwar, Mullana 133207, Haryana, India*
[2]*Department of Chemistry, Indira Gandhi National College, Ladwa, Kurukshetra 136132, Haryana, India*
[3]*Department of Chemistry, Kurukshetra University, Kurukshetra 136119, Haryana, India*

✉*Corresponding author: parveen.gupta@mmumullana.org;* ORCID: https://orcid.org/0000-0002-2718-1310

Received: 06 August 2025; revised: 02 November 2025; accepted: 10 December 2025

## ABSTRACT

New copper, manganese and vanadium based heterogeneous catalysts have been developed by the immobilization of pyridyl benzimidazole onto the polymer support. The active catalysts were characterized using CHN, FT-IR, DRS, EPR, AAS and EDX techniques and successfully used for the oxidative transformation of ethyl benzene. Metal loading in mmol per gram of resin in different catalysts was found to be 0.94-1.34. The catalytic potential of the synthesized catalysts was evaluated for the oxidation of ethylbenzene using hydrogen peroxide and tert-butyl hydroperoxide as oxidant with undiminished efficiency profiles and good reusability (up to four cycles). Notably, no metal contamination in the final products was observed. The comparative evaluation revealed that the highest percentage conversion (82.8 %) and highest selectivity (82.5) for benzaldehyde formation was attained with manganese as catalyst using $H_2O_2$ as an oxidant. The mechanism of the oxidation of ethylbenzene in the presence of catalyst has also been proposed. The developed catalytic systems are operationally simple and environmentally clean.

**Keywords:** Heterogeneous catalyst, recyclability, chloromethylated polystyrene, ethylbenzene, 2-(2-pyridyl) benzimidazole, oxidants, selectivity.

## INTRODUCTION

In context to modern ecosystem the development of efficient and sustainable catalytic systems for the oxidation of hydrocarbons, such as ethylbenzene, is of paramount importance in both industrial and environmental contexts [1]. Traditional oxidation methods often suffer from drawbacks such as harsh reaction conditions, low selectivity, and the use of environmentally harmful oxidants [2]. Consequently, there is a growing demand for catalysts that can operate under mild conditions, exhibit high selectivity, and are environmentally benign [3]. In this regard, supported catalysts have emerged as a promising class of catalysts, combining the advantages of homogeneous catalysis, such as high activity and selectivity, with the stability and recyclability of heterogeneous systems [4]. Chloromethylated polymers, in particular, have gained significant attention as versatile supports due to their ease of functionalization and ability to anchor a wide range of ligands and metal centres [5-6]. When paired with redox-active transition metals, these polymer-supported systems exhibit enhanced catalytic performance in various chemical transformations like oxidation [7-8], hydrogenation [9], esterification [10], carbonylation [11], olefinations [12], olefin metathesis [13], isomerisation [14], cross coupling reactions [15] etc. The 2-(2-pyridyl) benzimidazole ligand [16-17], known for its strong chelating ability and stability, has been widely used to form well-defined complexes with diverse catalytic applications. By supporting 2-(2-pyridyl) benzimidazole based complexes onto chloromethylated polymers, it is possible to create robust and recyclable catalysts with tailored properties for oxidation reactions. This research focuses on the synthesis of new immobilized 2-(2-pyridyl) benzimidazole based metal catalysts. The study aims to explore the structural and spectroscopic characteristics of these catalysts, as well as their catalytic efficiency, selectivity, and reusability in the oxidative transformation of ethylbenzene. By utilizing the synergistic effects of the 2-(2-pyridyl) benzimidazole ligand, the redox-active metal centres, and the polymer support, this work

seeks to develop a sustainable and efficient catalytic system for the oxidation of aromatic hydrocarbon. The oxidation of ethylbenzene in the presence of catalyst can produce a range of products, including benzaldehyde, acetophenone and phenylacetic acid as a major product [18-19]. Benzaldehyde is a versatile organic compound with a distinctive odor and a wide range of applications across various industries. It is the simplest aromatic aldehyde and serves as a key intermediate in the synthesis of numerous chemicals, widely used as a flavoring agent in foods and beverages due to its characteristic almond-like aroma and also finds uses as a key component in almond extracts [20]. Acetophenone is an important organic compound with several applications in various industries. It is primarily known for its use as a flavoring agent, fragrance, and intermediate in chemical synthesis [21]. Phenylacetic acid is used in the synthesis of several pharmaceuticals, it is a precursor in the production of some β-lactam antibiotics like penicillin and ampicillin, which are critical for treating bacterial infections, used in drug formulations and synthesizing compounds for anti-inflammatory, anticancer, and other therapeutic purposes [22].

## EXPERIMENTAL

***Materials and instruments:*** Chloromethylated polystyrene (crosslinked with divinylbenzene) was obtained as gift from Thermax Chemical Limited Pune. 2-(2-pyridyl) benzimidazole (Sigma-aldrich); vanadyl sulphate pentahydrate, copper chloride dihydrate, manganese acetate tetrahydrate, silver nitrate, dimethylformamide, conc. nitric acid, hydrogen peroxide ($H_2O_2$, 30%), *tert*-butyl hydroperoxide (70%), acetonitrile, dimethylformamide, ethanol and methanol (CDH) were used for the synthesis. The Fourier Transform Infrared (FT-IR) spectra were recorded on Shimadzu IR spirit fourier transform infrared spectrophotometer. The diffused reflectance spectra (DRS) of the samples were recorded from UV-2600 Shimadzu double-beam spectrophotometer using $BaSO_4$ as the standard. Energy-dispersive X-ray analyses (EDX) spectra were recorded in FEG scanning electron microscope Hitachi SU8010 Series; CHNS were recorded on Thermo Scientific flash 2000; Metal analyses were performed on Shimadzu ASC-6880 atomic absorption spectrophotometer (AAS). EPR spectra were recorded on JES-FA200 X-band (9.45 GHz) spectrometer with a modulation frequency of 100 kHz. Modulation amplitude typically set at 2.0 Gauss, to maximize the signal without affecting resolution. GC-MS analysis were conducted on an Agilent 7000 GC/TQ system with a GsBP-624 column and Flame ionisation detector (FID) detector-equipped gas chromatograph.

***Functionalization of polystyrene resin with 2-(2-pyridyl) benzimidazole ($PSCH_2$-PBZ):*** The synthesis of the functionalized resin began by swelling 1 g of chloromethylated polystyrene in 20 mL of DMF at room temperature for 1 h. Separately, 4.5 mmol of 2-(2-pyridyl) benzimidazole was dissolved in 20 mL of DMF and subsequently added to the pre-swollen polymer suspension. Upon addition, the solution's color rapidly changed to light yellow. To facilitate the reaction, 0.7 mL of triethylamine was introduced, and the mixture was refluxed under stirring at 80 °C for 8 h. After completion, the reaction mixture was allowed to cool to room temperature, followed by vacuum filtration. The product was thoroughly washed multiple times with hot DMF and hot ethanol to remove any unreacted residues. Finally, the functionalized resin was dried in an air oven at 80 °C.

***Loading of metal (V/Mn/Cu) on functionalized resin:*** 1.0 g sample of $PSCH_2$-PBZ was swelled in 10 mL of DMSO for 1 h. A solution of $CuCl_2 \times 2H_2O$/ $VOSO_4 \times 5H_2O$/ $Mn(CH_3COO)_2 \times 4H_2O$ (4.5-9.0 mmol) was prepared in DMSO and subsequently added to the swelled polymer suspension. As the reaction progressed, a noticeable change in the resin's color was observed. The mixture was then refluxed under continuous stirring for 6 h. After completion, the resin was allowed to cool to room temperature, followed by vacuum filtration. It was then thoroughly washed multiple times with hot DMSO and hot ethanol to remove any unreacted species. Finally, the purified metal loaded resin was dried in an oven at 80 °C.

***Catalytic oxidation reaction:*** The oxidation reaction was performed in a thermostatted oil bath using a round-bottom flask. The catalyst was pre-swollen in acetonitrile (20 ml) for 30 minutes before adding ethylbenzene (10 mmol), an oxidant (20 mmol), and the catalyst (0.1–0.15 g). The mixture was refluxed and the reaction was primarily examined on TLC under the varying conditions such as catalyst amount, oxidant type (TBHP, $H_2O_2$), temperature, and duration (4–8 h). The products were confirmed by GC-MS.

## RESULTS AND DISCUSSION

The crosslinked polystyrene resin was functionalized with 2-(2-pyridyl) benzimidazole using triethylamine and DMF, forming [$PSCH_2$-PBZ] Scheme 1. Ligand attachment was confirmed by heating the beads with pyridine, followed by nitric acid and silver nitrate, where no white precipitate indicated chlorine replacement. The ligand's para-position attachment is shown in Fig. 1. Metal loading onto the functionalized resin (Scheme 2) was initially confirmed by a color change and later by spectroscopic analysis.

***Characterization:*** Elemental data for the functionalised resin and its metal catalysts are presented in Table 1. Metal content was determined experimentally by acid leaching of 0.1 gm of the catalyst for 3 h followed by AAS determination. The experiments were performed at least three times, and the mean values are reported in Table 1. Ligand incorporation was calculated from %N obtained from CHN analyser.

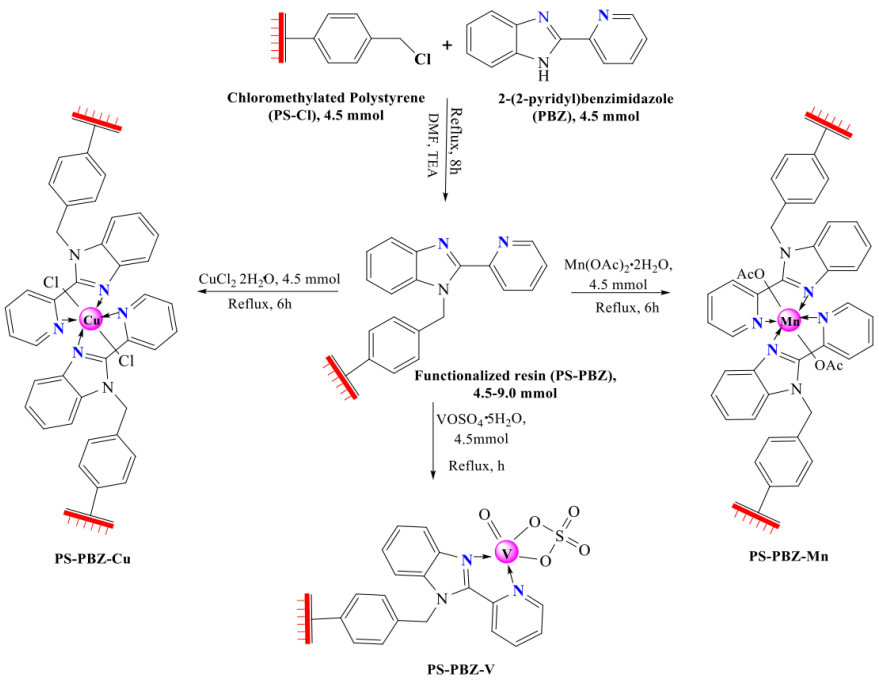


Scheme 1. Synthesis of functionalized resin and its metal catalyst

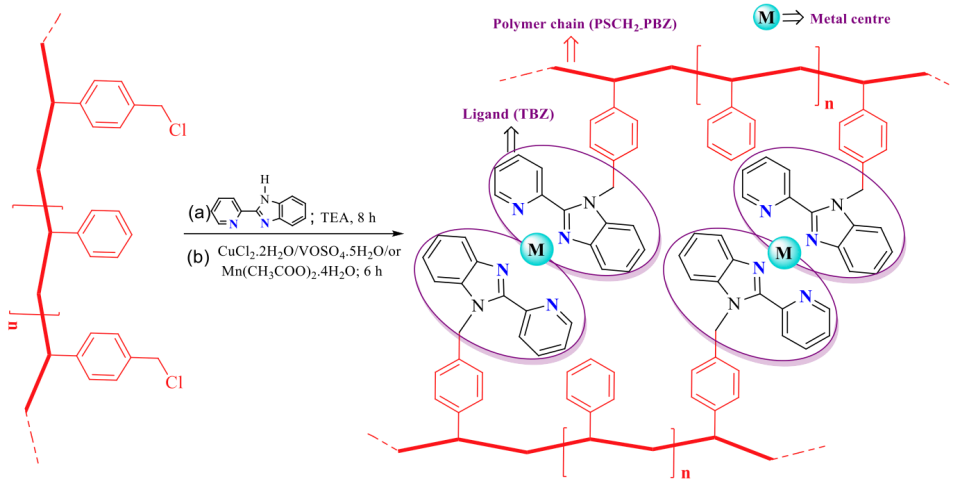


Fig. 1. Picture illustrating the metal loaded polystyrene beads (neglecting the cross-linking with divinylbenzene)

Table 1. Analytical data of $PSCH_2$-PBZ and its metal catalyst

| | Colour | Elemental analysis (%) | | | | | Ligand incorporation (mmol/g) | Metal incorporation (mmol/g) (Mean of triplicates) | Ligand: Metal ratio |
|---|---|---|---|---|---|---|---|---|---|
| | | C | H | N | S | M | | | |
| [$PSCH_2$-PBZ] | off white | 82.52 | 7.17 | 10.31 | | | 2.45 | | |
| [$PSCH_2$-PBZ-V] | light green | 60.38 | 5.02 | 7.01 | 5.77 | 6.81 | 1.67 | 1.37, 1.32, 1.33 → 1.34 | 1.2:1 |
| [$PSCH_2$-PBZ-Mn] | brown | 72.82 | 6.32 | 8.64 | | 5.65 | 2.05 | 1.05, 1.03, 1.01 → 1.03 | 1.9:1 |
| [$PSCH_2$-PBZ-Cu] | light yellow | 71.89 | 5.93 | 8.80 | | 5.97 | 2.1 | 0.92, 0.94, 0.96 → 0.94 | 2.2:1 |

Ligand incorporation (mmol/g) = % N × 100 ÷ (14 × n)

where n is the number of nitrogen atoms per ligand. Metal incorporation was calculated using the formula:

Metal incorporation (mmol/g) = Observed metal % × 10 ÷ Atomic weight of metal

From these data, loading of ligand and metal onto the polystyrene resin was determined which helps in evaluating the ligand to metal stoichiometry.

The successful attachment of the ligand onto the polystyrene resin, followed by metal loading, was verified using EDX analysis Fig. 2. The spectrum of [$PSCH_2$-PBZ] (Fig. 2a) displays signals corresponding to C and N, confirming the ligand's incorporation with the polymer. The detection of metal ion signals across all catalysts indicates effective metal binding with [$PSCH_2$-PBZ]. The EDX spectrum of [$PSCH_2$-PBZ-V] (Fig. 2b) displays characteristic signals corresponding to C, N, O, S, and V elements. The presence of oxygen and sulphur peaks confirms the coordination of sulphate group to the metal centre. The [$PSCH_2$-PBZ-Mn] (Fig. 2c) catalyst exhibits signals due to C, N, O, and Mn, where the oxygen signal supports the coordination of acetate group. Similarly, the EDX spectrum of [$PSCH_2$-PBZ-Cu] (Fig. 2d) shows peaks for C, N, Cl, and Cu, and the presence of chlorine indicates the coordination of chloride ions with the copper centre.

***FT-IR study:*** The overlay spectra of the synthesized compounds are presented in Fig. 3, while Table 2 summarizes the key vibrational bands observed for the supported 2-(2-pyridyl) benzimidazole [$PSCH_2$-PBZ] and its corresponding metal catalysts.

In the spectrum of [$PSCH_2$-PBZ], the absorption bands at 1680 $cm^{-1}$ and 1264 $cm^{-1}$ can be attributed to the stretching vibrations of the $\nu$ (C=N) (imi + py) bonds (from both imidazole and pyridine rings) and the C-N bond, respectively. A comparative analysis of the FT-IR spectra of [$PSCH_2$-PBZ] and its catalysts indicates that the ligand coordinates to the metal ions in a bidentate manner. This is evident from the significant shifts in the C=N stretching frequencies, which vary by approximately 8-16 $cm^{-1}$ in the metal complexes, confirming the involvement of nitrogen atoms in coordination [23]. However, the C-N stretching frequency in the polymer-supported ligand remains largely unchanged upon metal coordination. Further evidence of metal binding is provided by the appearance of new bands in the metal catalysts, corresponding to metal-nitrogen (M-N), metal-oxygen (M-O), and metal-chlorine (M-Cl) interactions. These bands are observed in the regions of 469-481 $cm^{-1}$, 518-539 $cm^{-1}$, and 365 $cm^{-1}$, respectively. In the case of [$PSCH_2$-PBZ-Mn], distinct bands at 1548 $cm^{-1}$ and 1373 $cm^{-1}$ can be linked to the asymmetric and symmetric stretching vibrations of the acetate (OAc) groups, suggesting their monodentate coordination and supporting the covalent nature of the metal-oxygen bond [24]. Additionally, in [$PSCH_2$-PBZ-V], a characteristic band at 971 $cm^{-1}$ confirms the presence of a V=O stretching mode [25]. Furthermore, absorption band observed at 1120 $cm^{-1}$ and 1035 $cm^{-1}$ is associated with bidentate sulfate coordination, as indicated by the asymmetric and symmetric stretching vibrations of the $SO_4$ group [26].

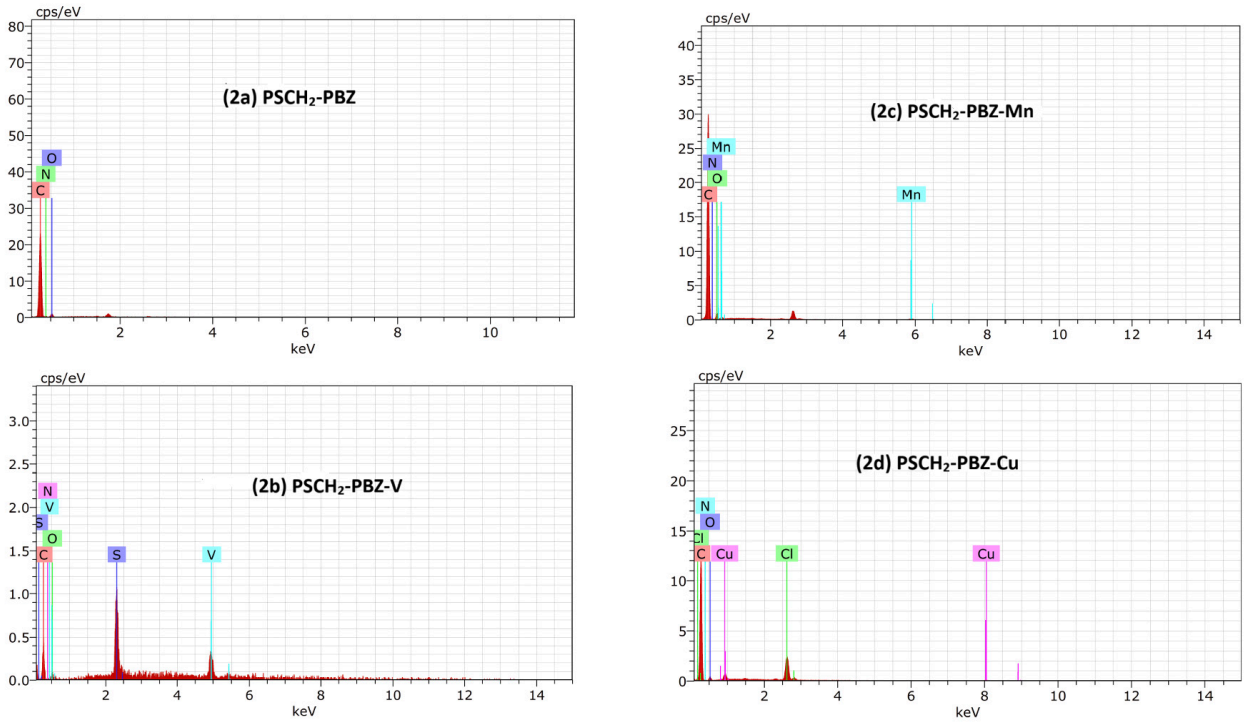


Fig. 2. EDX plot of functionalized polymer and polymer supported metal catalysts

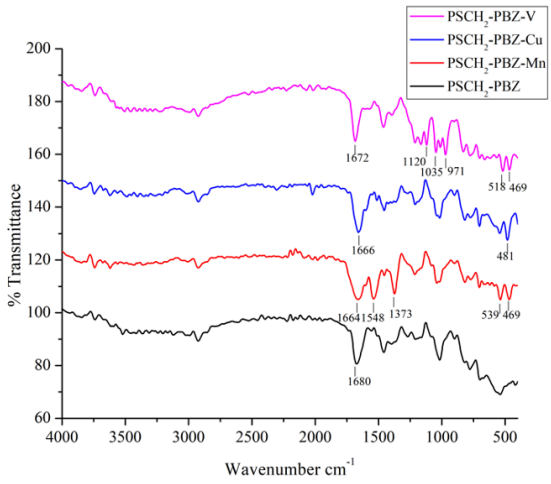


Fig. 3. Overlap spectra of functionalized polymer and polymer supported metal catalysts

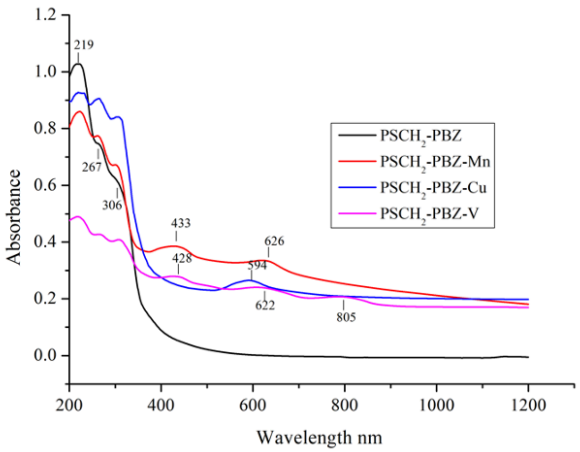


Fig. 4. Overlap DRS spectra of functionalized polymer its metal catalysts

Table 2. FTIR data for the $PSCH_2$-TBZ and its complexes

| Polymer-supported compounds | ν (C=N) (imi+ py) | ν (C-N) | $\nu_{sy}$(OAc)/ $\nu_{asy}$(OAc) | $\nu_{sy}$($SO_4$)/ $\nu_{asy}$($SO_4$) | ν (V=O) | ν (M-N) | ν (M-O) | ν (M-Cl) |
|---|---|---|---|---|---|---|---|---|
| [$PSCH_2$-PBZ] | 1680 | 1264 | | | | | | |
| [$PSCH_2$-PBZ-V] | 1672 | 1262 | | 1120, 1035 | 971 | 469 | 518 | |
| [$PSCH_2$-PBZ-Mn] | 1664 | 1263 | 1548,1373 | | | 469 | 539 | |
| [$PSCH_2$-PBZ-Cu] | 1666 | 1264 | | | | 481 | | 365 |

***Diffused reflectance spectra:*** The diffused reflectance spectroscopy (DRS) analysis was conducted (Table 3 and Fig. 4) to investigate the electronic transitions and coordination environments of the catalysts. This technique provided information to confirm the oxidation states and geometries of the metal centres. The DRS spectrum of the ligand-functionalized polymer exhibited distinct absorption bands at 45662, 38167 and 32680 $cm^{-1}$, corresponding to φ → φ*, π → π*, n → π* transitions within the 2-(2-pyridyl) benzimidazole ligand. These bands remained present in the metal-loaded catalysts, with slight shifts, indicating successful coordination of the metal centers without significant alteration of the polymer's electronic structure. The vanadium-supported catalyst displayed three well-defined d-d transition bands at 12422; 16077 and 24331 $cm^{-1}$. These transitions were characteristic of a five-coordinate oxovanadium (IV) species in a square pyramidal ($C_{4V}$) geometry. The observed bands were assigned to the electronic transitions $^2B_2 \rightarrow {}^2E$, $^2B_2 \rightarrow {}^2B_1$ and $^2B_2 \rightarrow {}^2A_1$, consistent with previously reported spectral parameters for similar oxovanadium complexes [27, 28]. The manganese catalyst exhibited absorption bands at 15974 $cm^{-1}$ and 23094 $cm^{-1}$, corresponding to the spin-allowed $^2B_{1g} \rightarrow {}^2A_{1g}$, $^2B_{1g} \rightarrow {}^2B_{2g}$, $^2B_{1g} \rightarrow {}^2E_g$ transitions, respectively. These transitions confirmed the presence of high-spin Mn (II) in an octahedral ligand field [29, 30]. The copper catalyst exhibited a broad absorption band centred around 16835 $cm^{-1}$, indicative of multiple overlapping d-d transitions. These bands were assigned to $^2B_{1g} \rightarrow {}^2A_{1g}$, $^2B_{1g} \rightarrow {}^2B_{2g}$, $^2B_{1g} \rightarrow {}^2E_g$ transitions, which are characteristic of Cu (II) complexes in a distorted octahedral ($D_{4h}$) symmetry [29, 31]. The broad nature of the absorption band was attributed to Jahn-Teller distortion, a well-known effect in Cu (II) systems that influences their electronic structure.

Table 3. Diffused reflectance spectral data of functionalized resin and its metal catalysts

| Polymer supported metal catalysts | Transitions ($cm^{-1}$) | Band assignment |
|---|---|---|
| [$PSCH_2$-PBZ] | 45662, 38167, 32680 | φ→φ*, π→π*, n→π* |
| [$PSCH_2$-PBZ-V] | 12422, 16077, 24331 | $^2B_2 \rightarrow {}^2E$, $^2B_2 \rightarrow {}^2B_1$, $^2B_2 \rightarrow {}^2A_1$ |
| [$PSCH_2$-PBZ-Mn] | 15974, 23094 | $^6A_{1g} \rightarrow {}^4T_{1g}$(G), $^6A_{1g} \rightarrow {}^4T_{2g}$(G) |
| [$PSCH_2$-PBZ-Cu] | 16835 | $^2B_{1g} \rightarrow {}^2A_{1g}$, $^2B_{1g} \rightarrow {}^2B_{2g}$, $^2B_{1g} \rightarrow {}^2E_g$ |

***EPR study:*** The electron spin resonance (ESR) spectra (Fig. 5) of the vanadium and manganese catalysts were recorded at room temperature to gain insight into their electronic environments and coordination geometries. This technique provided valuable information regarding the oxidation states, ligand interactions, and overall structural properties of the metal centers

within the immobilized catalysts. The ESR spectrum of the vanadium-based catalyst displayed a distinct anisotropic signal characteristic of vanadyl species ($VO^{2+}$), confirming the presence of V(IV) in a square pyramidal coordination environment. The hyperfine splitting pattern, arising from the interaction between the unpaired electron and the vanadium nucleus (I = 7/2), resulted in an eight-line signal. The calculated g-values, $g_{\parallel}$ = 1.98 and $g_{\perp}$ = 2.0, along with the hyperfine coupling constants $A_{\parallel}$ = 178 G and $A_{\perp}$ = 80 G, were indicative of a typical $C_{4v}$ symmetry. The obtained spectral parameters confirmed that the vanadium centre was coordinated in a manner consistent with the expected oxovanadium complexes, with the V=O bond oriented along the principal axis [32, 33]. In the case of the manganese catalyst, the ESR spectrum exhibited a characteristic six-line hyperfine splitting pattern, typical of Mn (II) species (I = 5/2). The well-defined hyperfine interactions confirmed the presence of high-spin Mn (II) centers within the polymer framework. The g-value of g = 2.02 and hyperfine coupling constant A = 77 G suggested that the manganese ions were in an octahedral ligand field [34, 35]. The manganese catalyst displayed well resolved signal patterns due to spin-exchange interactions between neighboring Mn (II) centers, indicating a stable coordination environment without significant distortion.

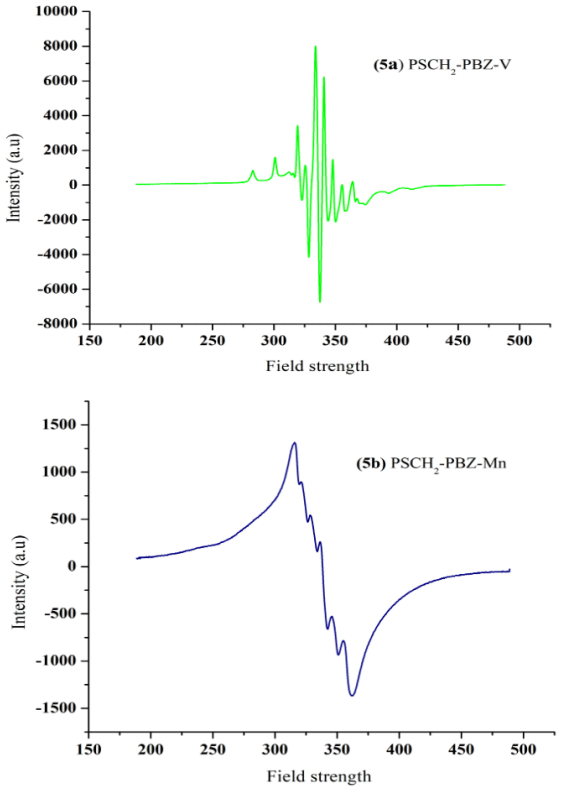


Fig. 5. EPR plot of [$PSCH_2$-PBZ-V] and [$PSCH_2$ PBZ-Mn]

***Catalytic activity:*** The catalytic efficiency of the synthesized polymer-supported metal catalysts was systematically assessed for the oxidation of ethylbenzene. The progress of the reaction was checked by taking small samples at different time intervals and analyzing them initially by TLC and finally by gas chromatography. The product selectivity and conversion of ethylbenzene were calculated using GC-MS. Each experiment w as repeated at least three times, and average values are reported. The conversion and selectivity values were obtained using the relative peak areas in the GC–MS chromatograms:

$$\% \text{ Conversion} = (\sum \text{area of all products} \div \sum \text{area of substrate} + \text{products}) \times 100$$

$$\% \text{ Selectivity} = (\text{Area of a particular product} \div \sum \text{area of all products}) \times 100$$

Samples of the solution were also tested for metal content at regular intervals. No metal was found in the solution, showing that the catalyst metal did not leach out during the reaction. After three reuse cycles, only a small decrease in metal content was observed. The study primarily focused on understanding the influence of different parameters, including oxidant type, reaction duration, temperature, and catalyst loading, to achieve optimal reaction conditions. Benzaldehyde was identified as the major product, accompanied by minor amounts of acetophenone and phenylacetic acid.

***Optimization of oxidants:*** To determine the most effective oxidant for the reaction, both hydrogen peroxide ($H_2O_2$) and tert-butyl hydroperoxide (TBHP) were employed under identical conditions. Control experiments performed in the absence of an oxidant confirmed that no significant conversion occurred, establishing the necessity of an oxidative environment. The results demonstrated that (Table 4, 5), $H_2O_2$ exhibited superior efficiency in acetonitrile in terms of percentage conversion (82.8%) and selectivity (82.5%) towards benzaldehyde, particularly in the presence of manganese-supported catalysts.

***Influence of reaction temperature:*** Temperature variation significantly impacted ethylbenzene oxidation. Experiments conducted between 40 °C to 80 °C revealed a direct correlation between temperature and conversion rate up to an optimal value of 65 °C. Beyond this temperature, peroxide decomposition increased, leading to reduced efficiency. Thus, 65 °C was identified as the ideal temperature for maximizing both conversion and selectivity.

***Effect of reaction time:*** The oxidation progress was monitored over time, revealing a gradual increase in ethylbenzene conversion. The reaction progress was monitored by conducting ethyl benzene reactions with TBHP/$H_2O_2$ in 1:2 ratio. An induction period of approximately 2 h was observed, followed by a steady increase in product formation. The highest conversion rates were achieved after 7 h (Fig. 6), with no significant

improvement beyond this point. Importantly, product selectivity remained consistent throughout extended reaction times, suggesting minimal side reactions.

***Catalyst loading and efficiency:*** The impact of catalyst concentration was evaluated by varying the catalyst amount from 0.1 g to 0.15 g, keeping the ethylbenzene and TBHP/or $H_2O_2$ conc. in 1:2 ratio, temperature 65 °C and time 4-8 h. The influence of the amount of catalyst on the oxidation of ethylbenzene as a function of time is shown in Table 4, 5 and Fig. 6a-6d. In the absence of a catalyst, only a negligible reaction was observed (6.2% to 12.8%). Increasing the catalyst concentration enhanced the conversion rate due to the greater availability of active sites. However, beyond 0.15 g, no substantial improvement was noted, indicating that saturation was reached.

Table 4. Conversion of ethylbenzene and product selectivity

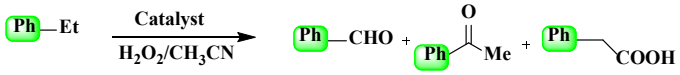


| Catalyst | Amount of catalyst (g) | Time (h) | Conversion (%) | Selectivity (%) | | | |
|---|---|---|---|---|---|---|---|
| | | | | Ph—CHO | Ph(C=O)Me | Ph—COOH | Others |
| Blank test | | 4 | 6.2 | 75.6 | 18.5 | 3.3 | 2.6 |
| | | 5 | 7.7 | 76.2 | 17.6 | 3.6 | 2.6 |
| | | 6 | 8.9 | 76.5 | 17.7 | 3.3 | 2.5 |
| | | 7 | 11.1 | 77.4 | 17.8 | 2.6 | 2.2 |
| | | 8 | 11.1 | 77.5 | 17.3 | 2.6 | 2.6 |
| [$PSCH_2$-TBZ-V] | 0.1 | 4 | 55.1 | 80.7 | 13.7 | 3.1 | 2.5 |
| | | 5 | 58.3 | 81.3 | 12.5 | 3.6 | 2.6 |
| | | 6 | 63.5 | 79.9 | 14.3 | 3.1 | 2.7 |
| | | 7 | 70.3 | 81.8 | 13.5 | 3.1 | 1.6 |
| | | 8 | 70.3 | 81.8 | 13.5 | 3.1 | 1.6 |
| | 0.15 | 4 | 56.2 | 81.7 | 12.4 | 3.5 | 2.4 |
| | | 5 | 59.9 | 80.4 | 14.7 | 3.6 | 1.3 |
| | | 6 | 67.2 | 79.1 | 13.9 | 4.0 | 3.0 |
| | | 7 | 74.4 | 80.2 | 12.7 | 4.8 | 2.3 |
| | | 8 | 74.4 | 80.2 | 12.7 | 4.8 | 2.3 |
| [$PSCH_2$-TBZ-Mn] | 0.1 | 4 | 49.9 | 82.5 | 11.3 | 3.7 | 2.5 |
| | | 5 | 56.2 | 81.7 | 12.8 | 3.3 | 2.2 |
| | | 6 | 65.1 | 82.4 | 11.3 | 4.7 | 1.6 |
| | | 7 | 75.7 | 82.0 | 10.8 | 4.8 | 2.4 |
| | | 8 | 75.7 | 82.0 | 10.8 | 4.8 | 2.4 |
| | 0.15 | 4 | 56.1 | 80.8 | 12.2 | 5.8 | 1.6 |
| | | 5 | 68.7 | 82.5 | 10.2 | 4.9 | 2.5 |
| | | 6 | 73.6 | 80.9 | 11.1 | 5.8 | 2.4 |
| | | 7 | 82.8 | 80.0 | 11.8 | 4.6 | 3.6 |
| | | 8 | 82.8 | 80.0 | 11.8 | 4.6 | 3.6 |
| [$PSCH_2$-TBZ-Cu] | 0.1 | 4 | 42.0 | 75.5 | 17.7 | 4.6 | 2.2 |
| | | 5 | 45.2 | 76.8 | 18.7 | 3.4 | 1.1 |
| | | 6 | 49.5 | 75.6 | 17.1 | 4.7 | 2.6 |
| | | 7 | 52.8 | 74.4 | 18.8 | 4.8 | 2.0 |
| | | 8 | 52.8 | 74.4 | 18.8 | 4.8 | 2.0 |
| | 0.15 | 4 | 43.5 | 76.8 | 17.9 | 3.1 | 2.2 |
| | | 5 | 46.1 | 75.2 | 18.6 | 4.7 | 1.5 |
| | | 6 | 51.2 | 74.2 | 18.6 | 4.5 | 2.7 |
| | | 7 | 55.5 | 75.8 | 20.1 | 3.1 | 1.0 |
| | | 8 | 55.5 | 75.8 | 20.1 | 3.1 | 1.0 |

Reaction conditions: $CH_3CN$ (20 ml), Ethylbenzene (10 mmol), $H_2O_2$ (20 mmol), Temperature (65 °C); Conversion refers to GCMS analysis.

Table 5. Conversion of ethylbenzene and product selectivity

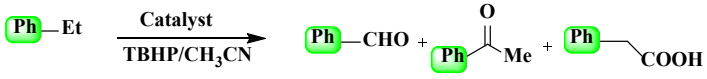


| Catalyst | Amount of catalyst (g) | Time (h) | Conversion (%) | Selectivity (%) | | | |
|---|---|---|---|---|---|---|---|
| | | | | Ph—CHO | Ph(C=O)Me | Ph—COOH | Others |
| Blank test | | 4 | 6.5 | 72.6 | 19.5 | 4.2 | 2.7 |
| | | 5 | 7.9 | 70.8 | 20.5 | 4.2 | 2.7 |
| | | 6 | 10.9 | 70.6 | 20.2 | 4.8 | 2.4 |
| | | 7 | 12.8 | 71.8 | 18.9 | 3.6 | 1.6 |
| | | 8 | 12.8 | 71.8 | 18.9 | 3.6 | 1.6 |
| [$PSCH_2$-TBZ-V] | 0.1 | 4 | 35.7 | 72.7 | 17.1 | 7.4 | 2.8 |
| | | 5 | 43.8 | 74.3 | 17.0 | 6.4 | 2.3 |
| | | 6 | 46.2 | 72.2 | 18.2 | 6.2 | 3.4 |
| | | 7 | 50.2 | 77.1 | 15.1 | 5.6 | 2.2 |
| | | 8 | 50.2 | 77.1 | 15.1 | 5.6 | 2.2 |
| | 0.15 | 4 | 37.8 | 69.5 | 20.6 | 7.4 | 2.5 |
| | | 5 | 44.5 | 71.5 | 18.6 | 7.6 | 2.3 |
| | | 6 | 50.7 | 72.0 | 20.5 | 5.0 | 2.5 |
| | | 7 | 55.6 | 71.4 | 19.6 | 6.5 | 2.5 |
| | | 8 | 55.6 | 71.4 | 19.6 | 6.5 | 2.5 |
| [$PSCH_2$-TBZ-Mn] | 0.1 | 4 | 48.9 | 78.5 | 12.4 | 5.4 | 3.7 |
| | | 5 | 55.8 | 80.3 | 11.2 | 6.2 | 2.3 |
| | | 6 | 59.2 | 78.5 | 10.5 | 8.1 | 2.9 |
| | | 7 | 68.6 | 78.6 | 11.5 | 7.5 | 2.4 |
| | | 8 | 68.6 | 78.6 | 11.5 | 7.5 | 2.4 |
| | 0.15 | 4 | 50.9 | 79.3 | 10.6 | 6.5 | 3.6 |
| | | 5 | 58.9 | 78.5 | 12.6 | 6.6 | 2.3 |
| | | 6 | 64.6 | 77.3 | 12.9 | 6.4 | 3.4 |
| | | 7 | 72.2 | 78.9 | 12.8 | 6.1 | 2.2 |
| | | 8 | 72.2 | 78.9 | 12.8 | 6.1 | 2.2 |
| [$PSCH_2$ TBZ-Cu] | 0.1 | 4 | 48.6 | 71.5 | 17.8 | 7.7 | 3.1 |
| | | 5 | 53.3 | 73.5 | 16.3 | 7.4 | 2.8 |
| | | 6 | 55.4 | 72.2 | 16.5 | 8.9 | 2.4 |
| | | 7 | 60.8 | 73.4 | 15.7 | 8.7 | 2.2 |
| | | 8 | 60.8 | 73.4 | 15.7 | 8.7 | 2.2 |
| | 0.15 | 4 | 52.7 | 73.6 | 15.5 | 8.5 | 2.4 |
| | | 5 | 55.1 | 74.7 | 14.6 | 7.3 | 3.4 |
| | | 6 | 62.8 | 74.7 | 14.6 | 7.4 | 3.3 |
| | | 7 | 64.8 | 73.8 | 15.4 | 8.3 | 2.5 |
| | | 8 | 64.8 | 73.8 | 15.4 | 8.3 | 2.5 |

Reaction conditions: $CH_3CN$ (20 ml), Ethylbenzene (10 mmol), $H_2O_2$ (20 mmol), 0.15 g catalyst, Temperature (65 °C); Time (7 h) Conversion refers to GCMS analysis.

***Catalyst reusability:*** A crucial aspect of heterogeneous catalysis is catalyst recyclability. After each reaction cycle, the catalysts were recovered, washed, and reused under identical conditions. From the Table 6 and Fig. 7, it can be observed that, performance remained largely unchanged over three consecutive cycles, with only a slight decrease observed after the fourth cycle due to loss of metal content. Structural integrity was confirmed through spectroscopic analysis, and atomic absorption spectroscopy (AAS) revealed minimal metal leaching, ensuring the catalysts' stability.

***Plausible mechanism:*** Scheme 2 shows the mechanism [36] for the oxidation of ethylbenzene in presence peroxide ($H_2O_2$/TBHP) and catalyzed by metal catalyst. Firstly, metal catalyst in presence of peroxide forms active hydroperoxide species leaving

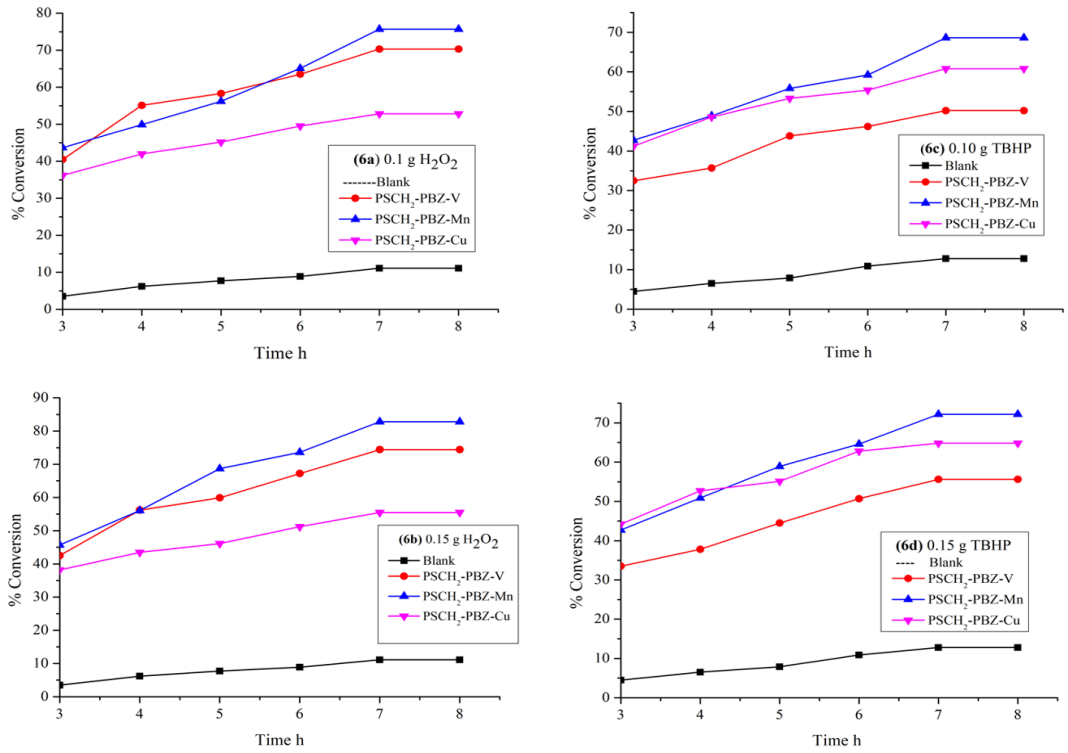


Fig. 6. Study of time variation on ethylbenzene oxidation with immobilized catalysts

Table 6. Recyclability test

| Catalyst | Cycle | Conversion (%) | Selectivity (%) | | | |
|---|---|---|---|---|---|---|
| | | | Ph—CHO | Ph, O, Me | Ph—COOH | Others |
| [$PSCH_2$-TBZ-V] | 1 | 74.4 | 80.2 | 12.7 | 4.8 | 2.3 |
| | 2 | 74.4 | | | | |
| | 3 | 74.4 | | | | |
| | 4 | 74.1 | | | | |
| | 5 | 72.2 | | | | |
| [$PSCH_2$-TBZ-Mn] | 1 | 82.8 | 80.0 | 11.8 | 4.6 | 3.6 |
| | 2 | 82.8 | | | | |
| | 3 | 82.8 | | | | |
| | 4 | 82.5 | | | | |
| | 5 | 79.2 | | | | |
| [$PSCH_2$-TBZ-Cu] | 1 | 55.5 | 75.8 | 20.1 | 3.1 | 1.0 |
| | 2 | 55.5 | | | | |
| | 3 | 55.5 | | | | |
| | 4 | 55.1 | | | | |
| | 5 | 52.2 | | | | |

Reaction conditions: $CH_3CN$ (20 ml), Ethylbenzene (10 mmol), $H_2O_2$ (20 mmol), 0.15 g catalyst, Temperature (65 °C); Time (7 h) Conversion refers to GCMS analysis.

out chloride ion/acetate ion. The benzylic carbocation is stabilized by resonance, allowing a nucleophilic attack by the *tert*-butylperoxide anion to generate phenyl ethanol which further undergoes rearrangement and cleavage of peroxide bond to yield benzaldehyde and acetophenone.

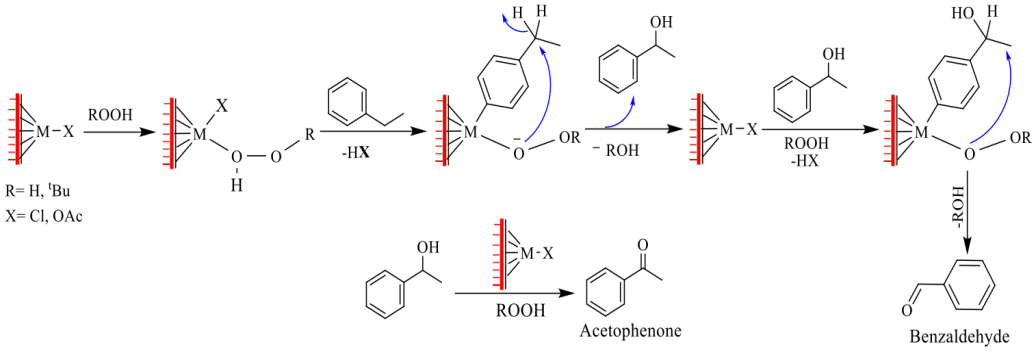


Scheme 2. Proposed mechanism for the $H_2O_2$/TBHP mediated oxidation of ethylbenzene catalysed by supported metal catalyst

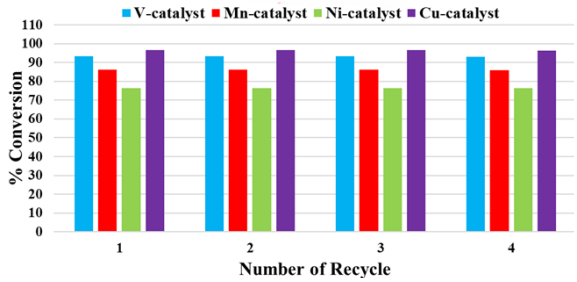


Fig. 7. Recycling performance of polystyrene-bound metal catalyst

## CONCLUSION

This study focuses on the synthesis and catalytic application of immobilized 2-(2-pyridyl)benzimidazole metal complexes for the efficient liquid phase oxidation of ethylbenzene. The catalysts were prepared by covalently anchoring 2-(2-pyridyl)benzimidazole onto a chloromethylated polystyrene support, followed by the incorporation of Cu (II), V (IV), and Mn (II) metal ions. Under optimized reaction conditions (0.15 g catalyst, 65 °C, 7 h) and using hydrogen peroxide as an oxidant, the catalysts exhibited significant activity for ethylbenzene oxidation. Among the primary oxidation products- benzaldehyde, acetophenone, and phenylacetic acid,benzaldehyde was identified as the most selectively formed product. The conversion efficiency and benzaldehyde selectivity in the presence of $H_2O_2$ followed the order Mn (82.8%) > V (74.4%) > Cu (55.5%) and Mn (82.5) > V (81.8) > Cu (76.5), respectively. When tert-butyl hydroperoxide (TBHP) was used as the oxidant, the conversion rates and selectivity followed Mn (72.2%) > Cu (64.8%) > V (55.6%) and Mn (80.3) > V(77.1) > Cu(74.7), respectively. Overall, the manganese-based catalyst emerged as the most effective in terms of both conversion rate and selectivity. This research underscores the potential of polymer-supported catalysts as efficient and reusable systems for ethylbenzene oxidation. Further investigations could explore their application in broader catalytic transformations while optimizing conditions for industrial scalability and environmental sustainability.

## FUNDING

This work was supported by ongoing institutional funding. No additional grants to carry out or direct this particular research were obtained.

## CONFLICTS OF INTEREST

The authors declare no conflict of interest.

## REFERENCES

1. Rahman M.M., Ara M.G., Rahman M.S., *et al.* (2020) Recent development of catalytic materials for ethylbenzene oxidation. *Journal of Nanomaterials*, **1**, 7532767. https://doi.org/10.1155/2020/7532767
2. Bäckvall J.E. (Ed.) (2011) Modern oxidation methods, John Wiley & Sons.
3. He C., Cheng J., Zhang X., et al. (2019) Recent advances in the catalytic oxidation of volatile organic compounds: a review based on pollutant sorts and sources. *Chemical reviews*, **119(7)**, 4471-4568. https://doi.org/10.1021/acs.chemrev.8b00408
4. Poovan F., Chandrashekhar V.G., Natte K., *et al.* (2022) Synergy between homogeneous and heterogeneous catalysis. *Catalysis Science & Technology*, **12(22)**, 6623. https://doi.org/10.1039/D2CY00232A
5. Khokhar D., Kour M., Phu, R., *et al.* (2024) Polystyrene-supported catalysts. *Polymer Supported Organic Catalysts*, CRC Pres, *pp*. 89-100.
6. Kumari S., Kumar S., Karan R., *et al.* (2024) Synthetic and catalytic perspectives of polystyrene supported metal catalyst. *Journal of the Iranian Chemical Society*, **21(4)**, 951. https://doi.org/10.1007/s13738-024-02970-7
7. Kargar H., Moghada M., Shariati, L., *et al.* (2022) Novel oxo–peroxo W (VI) Schiff base complex: Synthesis, SC-XRD, spectral characterization, supporting on chloromethylated polystyrene, and catalytic oxidation of sulfides. *Journal of the*

*Iranian Chemical Society*, **19(7)**, 3067-3077. https://doi.org/10.1007/s13738-022-02517-8
8. Maurya M.R., Patter A., Chauhan A., *et al*. (2024) Dioxidomolybdenum (VI) complex supported on chloromethylated polymer and its catalytic role in peroxidase mimicking activity towards oxidation of dopamine. *Topics in Catalysis*, **67(5)**, 466-482. https://doi.org/10.1007/s11244-023-01861-0
9. Sharma A.S., Sharma V.S., Yadav P., *et al.* (2023) Polystyrene resins: Versatile and economical support for heterogeneous nanocatalysts in sustainable organic reactions. *Chem. Cat. Chem.*, **15(8)**, e202201493. https://doi.org/10.1002/cctc.202201493
10. Chakravarthy A.J., Madhura M.J., Gayathri V. (2024) A Novel polymer supported copper (II) complex as reusable catalyst in oxidative esterification. *Catalysis Letters*, **154(2)**, 725. https://doi.org/10.1007/s10562-023-04337-8
11. Gautam P., Shah J.A., Bhanage B.M. (2023) Palladium-catalyzed carbonylation reactions in ionic liquids. *Encyclopedia of Ionic Liquids* (pp. 991-1004). Singapore: Springer Nature Singapore. https://doi.org/10.1007/978-981-33-4221-7_32
12. Dehbanipour Z., Moghadam M., Tangestaninejad S., *et al.* (2022) An efficient and selective olefination of aldehydes with ethyl diazoacetate using copper (II) bis-thiazole complex as heterogeneous catalyst. *Journal of the Iranian Chemical Society*, **19(8)**, 3371. https://doi.org/10.1007/s13738-022-02530-x
13. Suzuki N., Watanabe K., Takahashi C., *et al.* (2023) Ruthenium-catalyzed olefin metathesis in water using thermo-responsive diblock copolymer micelles, *Current Organic Chemistry*, **27(15)**, 1347. https://doi.org/10.2174/1385272827666230911115809
14. Bakhvalova E.S., Pinyukova A.O., Mikheev A.V., *et al.* (2021) Noble metal nanoparticles stabilized by hyper-cross-linked polystyrene as effective catalysts in hydrogenation of arenes. *Molecules*, **26(15)**, 4687. https://doi.org/10.3390/molecules26154687
15. Rajmane A., Mahey J., Kamble S., et al. (2024) In situ generated PdNPs immobilized on polystyrene supported DABCO dicationic ionic liquid: An efficient and reusable catalyst for Suzuki and Heck coupling reactions. *J. Organomet. Chem.*, **1022**, 123390. https://doi.org/10.1016/j.jorganchem.2024.123390
16. Chkirate K., Essassi E.M. (2022) Pyrazole and benzimidazole derivatives: chelating properties towards metals ions and their applications. *Current Organic Chemistry*, **26(19)**, 1735. https://doi.org/10.2174/1385272827666221216110504
17. Singha D., Halder S.C., Jana A.D., *et al.* (2024) The coordination chemistry and supramolecular interactions of 2-(2′-Pyridyl)imidazole ligand: A comprehensive review with theoretical insight. *Reviews in Inorganic Chemistry*, **44(2)**, 231. https://doi.org/10.1515/revic-2023-0016
18. Maurya M.R., Arya A., Adao P., *et al.* (2008) Immobilisation of oxovanadium (IV), dioxomolybdenum (VI) and copper (II) complexes on polymers for the oxidation of styrene, cyclohexene and ethylbenzene. *Applied Catalysis A: General*, **351(2)**, 239. https://doi.org/10.1016/j.apcata.2008.09.021
19. Renuka Maldepalli K., Virupaiah G., (2017) A polymer-anchored cobalt (II) complex as a reusable catalyst for oxidation of benzene, ethylbenzene and cyclohexane. *Trans. Met. Chem.*, **42**, 25. https://doi.org/10.1007/s11243-016-0102-z
20. Opgrande J.L., Dobratz C.J., Brown E., *et al.* (2000) Benzaldehyde. *Kirk-Othmer Encyclopedia of Chemical Technology*. https://doi.org/10.1002/0471238961.02051426151607 18.a01
21. Zubkov F.I., Kouznetsov V.V. (2023) Traveling across life sciences with acetophenone a simple ketone that has special multipurpose missions. *Molecules*, **28(1)**, 370. https://doi.org/10.3390/molecules28010370
22. Cook S.D. (2019) An historical review of phenylacetic acid. *Plant and Cell Physiology*, **60(2)**, 243. https://doi.org/10.1093/pcp/pcz004
23. Khalil M. M. H. (2000) $M(CO)_4$[2-(2'-pyridyl) benzimidazole] complexes; M = Mo or W. *Trans. Met. Chem.*, **25(3)**, 358–360. https://doi:10.1023/a:1007001003628
24. Tuna M., Ugur T. (2022) Synthesis of novel of Mn (II), Co (II), and Cu (II) Schiff base complexes and their high catalytic effect on bleaching performance with $H_2O_2$, *J. Mol. Struct.* **1265**, 133348. https://doi.org/10.1016/j.molstruc.2022.133348
25. Sharma B. P., Subin J. A., Marasini B. P., *et al.* (2023) Triazole based Schiff bases and their oxovanadium (IV) complexes: Synthesis, characterization, antibacterial assay, and computational assessments. *HeliyonI.* **9(4)**, 1. https://doi.org/10.1016/j.heliyon.2023.e15239
26. Singh V. P., Singh S., Katiyar A. (2009) Synthesis, physico-chemical studies of manganese (II), cobalt (II), nickel (II), copper (II) and zinc (II) complexes with some p-substituted acetophenone benzoylhydrazones and their antimicrobial activity. *J. Enzyme Inhib. Med. Chem*, **24(2)**, 577. https://doi:10.1080/14756360802318662
27. Sahani M.K., Yadava U., Pandey O.P., *et al.* (2014) *Spectrochim. Acta A Mol. Biomol. Spectrosc*., **125**, 189. https://doi:10.1016/j.saa.2014.01.041
28. Renuka M.K., Gayathri V. (2019) Oxidation of benzyl alcohols by polymer supported V(IV) complex using $O_2$. *Catal. Lett.* **149**, 1266–1276. https://doi.org/10.1007/s10562-019-02710-0
29. Lupașcu G., Pahonțu E., Shova S., *et al.* (2021) Co (II), Cu (II), Mn (II), Ni (II), Pd (II), and Pt (II) complexes of bidentate Schiff base ligand:

Synthesis, crystal structure, and acute toxicity evaluation. *Appl. Organomet. Chem.*, **35(4)**, 1. https://doi.org/10.1002/aoc.6149

30. Chandra S., Gupta L.K. (2004) EPR, IR and electronic spectral studies on Mn(II), Co(II), Ni(II) and Cu(II) complexes with a new 22-membered azamacrocyclic [$N_4$] ligand. *Spectrochimica Acta Part A: Molecular and Biomolecular Spectroscopy* **60**(8-9), 1751-1761. https://doi.org/10.1016/j.saa.2003.07.011
31. Singh Y.P., Patel R.N., Singh Y., *et al.* (2016) Structure and antioxidant superoxide dismutase activity of copper (II) hydrazone complexes. *Polyhedron*. **122**(28), 1-15. http://dx.doi.org/10.1016/j.poly.2016.11.013
32. Krzystek J., Ozarowski A., Telser J., et al. (2015) High-frequency and -field electron paramagnetic resonance of vanadium (IV, III, and II) complexes. *Coord. Chem. Rev.*, 301-302, 123–133. https://doi:10.1016/j.ccr.2014.10.014
33. Mahboubi-Anarjan P., Bikas R., Hosseini-Monfared H., *et al.* (2017) Synthesis, characterization, EPR spectroscopy and catalytic activity of a new oxidovanadium (IV) complex with $N_2O_2$-donor ligand. *J. Mol. Struct.* **1131** 258-265. https://doi.org/10.1016/j.molstruc.2016.11.059
34. Hachuła B., Pędras M., Nowak M., *et al*. (2009) Synthesis, crystal structure, spectroscopic, and magnetic properties of a manganese (II) methoxyacetate complex [Mn($C_6O_6H_{10}$)($H_2O$)]n. *J. Coord. Chem.*, 63(1), 67. https://doi:10.1080/00958970903315535
35. Ali I.O., Nassar H.S., El-Nasser K.S., *et al.* (2021) Synthesis and characterization of Mn (II) and Co(II) complexes with poly(vinyl alcohol-nicotinic acid) for photocatalytic degradation of Indigo carmine dye. *Inorg Chem Commun*. **124**, 108360. https://doi.org/10.1016/j.inoche.2020.108360
36. Azeez M.O., Nafiu S.A., Olarewaju T.A., *et al.* (2023) Selective catalytic oxidation of ethylbenzene to acetophenone: A Review of catalyst systems and reaction mechanisms. *Ind. Eng. Chem. Res.*, **62**(33), 1. https://doi.org/10.1021/acs.iecr.3c01588